Electronic Conductivity of In_2O_3 Solid Solutions with ZrO_2

K. Sasaki,* H. P. Seifert, and L. J. Gauckler

Swiss Federal Institute of Technology (ETH-Zürich), Nichtmetallische Werkstoffe, CH-8092 Zürich, Switzerland

ABSTRACT

The electrical conductivity of In_2O_3-ZrO_2 as well as In_2O_3 solid solutions doped with SnO_2, CeO_2, Nb_2O_5, Pr_6O_{11}, and MgO is investigated, in the temperature range between room temperature and 1300°C, and in the oxygen partial pressure range between 5×10^{-5} and 1 atm. In_2O_3 doped with ZrO_2 is an electronic conductor, while ZrO_2 doped with In_2O_3 is an oxygen-ionic conductor. The two-phase material of the cubic (fcc) ZrO_2 + cubic (bcc) In_2O_3 solid solutions is a 3-dimensional composite of ionic and electronic conductors. The single-phase In_2O_3 doped with ZrO_2 is an electronic conductor with a conductivity up to 7×10^4 Sm^{-1} in air. Two maxima in electrical conductivity are found, one in the two-phase region and one in the In_2O_3 single-phase region. Lattice defects responsible for electronic conduction in pure and doped In_2O_3 are discussed. The defect models for In_2O_3 doped with ZrO_2 are proposed, and the Kröger-Vink diagram is constructed. The metastable solubility of dopants in In_2O_3 due to the slow phase separation kinetics influences the electronic conductivity. ZrO_2 is a most effective donor for increasing electronic conductivity of In_2O_3, among hypervalent metal oxides including SnO_2, Nb_2O_5, and CeO_2.

The In_2O_3-ZrO_2 system contains materials with both high oxygen-ion-conducting phases and a high electron-conducting phase, the amount of which can be varied to tailor the electrical conductivity for specific applications.[1,2] The phase diagram of this system has been revised previously.[1,2] The system includes the monoclinic, tetragonal, and cubic ZrO_2 solid solutions and the cubic In_2O_3 solid solution. The tetragonal- and cubic-ZrO_2 phases doped with In_2O_3 exhibit high ionic conductivities comparable to ZrO_2 doped with Y_2O_3.[2-6] The cubic-ZrO_2 phase, with $InO_{1.5}$ concentrations less than the cubic-ZrO_2 eutectoid composition of 23.5 mole percent (m/o), transforms to the tetragonal- (t′) ZrO_2 phase,[1,2,6-8] which affects ionic conductivity.[2] In the two-phase field of the cubic-ZrO_2 and the cubic-In_2O_3, electrical conductivities higher than 10^4 Sm^{-1} have been found at 1000°C.[9] ZrO_2 is a donor to increase electron concentration and electronic conductivity of In_2O_3.[10] In the cubic-In_2O_3 single-phase region, In_2O_3 doped with ZrO_2 exhibits a high n-type electronic conductivity,[9-12] similar to In_2O_3 doped with SnO_2 (ITO). SnO_2-doped In_2O_3 has been widely used as thin films for applications such as transparent electrodes, transparent heat reflectors, heterogeneous junction solar cells, protective conducting, or antistatic coating.[13-16]

In_2O_3 possesses the C-type rare-earth crystallographic structure.[17] This structure can be described as an oxygen-deficient fluorite structure, with twice the unit-cell edge of the corresponding fluorite cell, and with one quarter of the anions orderly missing.[18-24] Therefore, this structure is flexible in oxygen content, both for oxygen deficiency with oxygen vacancies, and for oxygen excess with oxygen interstitials.[18-24] In_2O_3 exhibits high oxygen diffusivity via oxygen vacancy in a reducing atmosphere, and via oxygen interstitial in an oxidizing atmosphere.[19,26-29] The ionic conductivity of In_2O_3 doped with SnO_2 was reported to be 0.5 Sm^{-1} even at temperatures as low as 1000 K.[29] Therefore doped-In_2O_3 is a mixed ionic-and-electronic conductor. Mixed-conducting oxides with high electronic conductivities are potentially interesting materials for electrode applications such as solid-oxide fuel-cell cathodes. The use of mixed conductors can reduce nonohmic polarization at the interface between the electrode and the electrolyte, and improves the performance of solid-oxide fuel cells.[30-35] In_2O_3 was one of the first materials applied as an air electrode for solid-oxide fuel cells.[36,37] The sublimation of In_2O_3 in a reducing atmosphere is reduced by doping with hypervalent metal oxides.[38]

Mixed-conduction, however, is not the only criterion for the electrode material selection. The electrode materials should be chemically compatible with the electrolyte, and no chemical reaction layer should be formed between the electrode and the electrolyte. One criterion for finding chemically and thermodynamically compatible cathode materials with ZrO_2-based electrolytes is to find a ZrO_2-metal oxide system, where an ion-conducting phase and an electron- (or mixed-) conducting phase can coexist.[39] Ideally, the metal oxide should be one of the stabilizer of the cubic-ZrO_2 phase with a high ionic conductivity, and ZrO_2 should be an excellent additive to the metal oxide for obtaining a high n- or p-type electronic or mixed conductivity. Many rare-earth sesquioxides as well as CaO and MgO are stabilizers of the cubic-ZrO_2 phase. Oxides with the rare-earth structure are In_2O_3 and Tl_2O_3, with a d^{10} outer electron configuration on the cation, Sc_2O_3, Y_2O_3 and many of the rare-earth oxides with a d^0 outer electron configuration on the cation.[24] In_2O_3 and Tl_2O_3, posttransition metal oxides, differ from the others in that the conduction band is a broad σ-type band, which may cause higher electronic conductivity than other rare-earth oxides.[24] Therefore the system In_2O_3-ZrO_2 system is a very limited system which includes an ion-conducting phase and an electron-conducting phase able to coexist in thermodynamic equilibrium to tailor a chemically compatible electronic conductor (cathode) with an ionic conductor (electrolyte). Thick films of ZrO_2-doped In_2O_3 have been prepared as cathode layers.[2,33,39,40] Chemically stable concentration-gradient cathode/electrolyte composites consisting of an ionic conductor, a mixed-conducting composite, and an electronic conductor have been prepared from this system by varying only the ratio of ZrO_2 and In_2O_3.[2]

Ionic and electronic conductivities, conduction mechanisms, and lattice defects should be understood, to use the In_2O_3-ZrO_2 system for various electrical, electrochemical, and optical applications. Our purpose therefore is to investigate electrical conductivity and lattice defect mechanisms in this system as functions of cation composition, temperature, oxygen partial pressure, as well as a kind of dopant. The system is also interesting for studying the effect of ionic radius on solubility, phase transformation, and defect association in zirconias,[1,2,4,7,8,41-43] and as hot-corrosion resistant thermal barrier coating material,[44] and as a base system for the $Ba_3In_2ZrO_8$ fast ionic conductor.[45]

*Electrochemical Society Active Member.

Downloaded on 2014-03-27 to IP 140.120.135.222 address. Redistribution subject to ECS terms of use (see ecsdl.org/site/terms_use) unless CC License in place (see abstract).

Experimental

All powders were prepared via wet-chemical coprecipitation, except the pure In_2O_3 powder. In_2O_3 (In_2O_3 > 99.99%,[a] PPM pure metals GmbH, Langelsheim, Germany) was dissolved in HCl solutions, and $ZrOCl_2$-$8H_2O$ (puriss, >99.0%, Fluka, Switzerland) as well as $SnCl_4$, $Ce(NO_3)_3$, $NbCl_5$, $MgCl_2$, $Pr(NO_3)_3$ was dissolved in distilled water. The appropriate mixtures of the two solutions were added to diluted NH_4OH solutions to obtain hydroxide precipitates. The precipitates were washed with distilled water and ethanol (puriss, >99.8%, Fluka, Switzerland), vacuum-filtered, and then calcined at 800°C for 1 h. Further details on powder preparation have been reported previously.[1,2]

The calcined oxide powders were uniaxially pressed at 50 MPa into pellets 16 mm in diam and 2 mm in thickness for x-ray diffraction (XRD) phase analysis, and into bars of dimensions 5 × 1.5 × 55 mm for 4-probe dc conductivity measurements. For pure In_2O_3 specimens, the starting high-purity In_2O_3 powder was directly taken to be pressed into the powder compacts. The specimens were sintered at 1500°C for 1 h, followed by furnace-cooling at a rate of 10°C/min. Additional specimens with 90 and 95 m/o $InO_{1.5}$-ZrO_2 were prepared and sintered at 1500°C for 12 and 36 h. Densities of all samples were more than 94% of theoretical. Special care has been taken to sinter the pure In_2O_3 specimens. Two specimens of 1 g were embedded in the same high purity In_2O_3 powder of 30 g in an Al_2O_3 crucible. Other specimens were sintered on powders with the corresponding composition, lying on ZrO_2-Y_2O_3 plates.

DC electrical conductivity was measured by 4-probe method using a microhmmeter (Keithley No. 580). The distance between the inner electrodes was 12 mm. Pt pastes (Degussa 308A) and pure Pt wires were used for electrical contacts. Electrical conductivity as a function of temperature was measured on cooling, from 1300°C to room temperature. The cooling rate was 4°C/min.

Isothermal electrical conductivity as a function of oxygen partial pressure (p_{O_2}) was measured in the p_{O_2} range between 5×10^{-5} and 1 atm, using O_2-Ar gas mixtures, with a flow rate of 280 ml/min, at 1300, 1150, and 1000°C. The specimens with $InO_{1.5}$ concentrations of 80, 95, 97.5, 99.5 m/o and pure In_2O_3 were selected for the study on the p_{O_2} dependence. Exact p_{O_2} was determined by measuring the electromotive force (EMF) using a ZrO_2-CaO tube. In each experimental condition, specimens were held at least for 2 h at 1300°C and for 6 h at 1150 and 1000°C. Conductivity data were obtained and regarded as in equilibrium with the atmosphere, when resistivity changed less than 1% during a further 1 h annealing. All temperatures were measured using Pt-10%Rh thermocouples, placed within 1 mm from specimens. EMF measurements were carried out to verify whether ionic or electronic conductivity is predominate, using air on the oxidizing side and O_2-Ar gas mixtures on the reducing side, with a Pt-electrode area of 1 cm^2.

Phase compositions were analyzed by x-ray diffraction (XRD, D5000, Siemens, Germany), using Cu-K_α radiation in the 2θ range between 20 and 80°. Microstructures of selected specimens (60, 70, and 80 m/o $InO_{1.5}$) were observed by scanning electron microscopy (SEM) (JEOL-6400) with an accelerating voltage of 27 kV.

Results

Electrical conductivity in the In_2O_3-ZrO_2 system.—The system possesses the monoclinic (m), tetragonal (t), and cubic (c) ZrO_2 solid solutions, and the cubic-In_2O_3 solid solution with the C-type rare-earth structure.[1,2] Figure 1 shows the electrical conductivity of In_2O_3-ZrO_2 as a function of $InO_{1.5}$ concentration at 1000°C. The ZrO_2 solid solution with In_2O_3 is an ionic conductor, and the In_2O_3 solid solution with ZrO_2 is an n-type electronic conductor. Electrical conductivity up to $InO_{1.5}$ concentrations of 45 m/o is of pure ionic character,[3] where the addition of In_2O_3 in ZrO_2 causes the formation of oxygen vacancies

$$In_2O_3 \xrightarrow{ZrO_2} 2In'_{Zr} + 3\,O_O^{\times} + V_O^{\bullet\bullet} \qquad [1]$$

in the Kröger-Vink notation.[47]

In materials with $InO_{1.5}$ concentrations of 50 m/o and higher, the conductivity is predominately of the electronic character. The doping of In_2O_3 with ZrO_2 causes electronic conductivity higher than 10^4 Sm^{-1}. In air, the maximum electrical conductivity was 7.0×10^4 Sm^{-1}, was found at 99.5 m/o $InO_{1.5}$ at 1300°C. The conductivities higher than 10^4 Sm^{-1} were observed in a wide concentration range from 70 to 99.5 m/o $InO_{1.5}$.

Three maxima in electrical conductivity were found in this system at 1000°C (*i*) at 25 m/o $InO_{1.5}$ near the cubic-ZrO_2 eutectoid composition, (*ii*) at 80 m/o $InO_{1.5}$ in the two-phase region of the cubic-ZrO_2 and the cubic-In_2O_3, and (*iii*) at 99.5 m/o $InO_{1.5}$ in the cubic-In_2O_3 single-phase region. The origin of the maximum at 25 m/o $InO_{1.5}$ has been discussed elsewhere.[2]

Electrical conductivity in the two-phase region: cubic-ZrO_2 + cubic-In_2O_3.—In the two-phase region of the cubic-ZrO_2 and the cubic-In_2O_3, the electrical conductivity increased abruptly with increasing $InO_{1.5}$ concentration from 50 m/o $InO_{1.5}$, as shown in Fig. 1. The electrical conductivity at 1000°C reached 4×10^4 Sm^{-1} at 80 m/o $InO_{1.5}$. EMF measurements of the 80 m/o $InO_{1.5}$-ZrO_2 with O_2-Ar mixtures against air revealed that the ionic transference number was on the order of 10^{-4}, indicating that electronic conductivity rather than ionic conductivity is predominate in the two-phase material.

To study the distribution of both phases, microstructural observations of 60, 70, and 80 m/o $InO_{1.5}$-ZrO_2, were made by SEM. The micrograph of the 80 m/o specimen before HCl etching and the micrographs of the 60, 70, and 80 m/o specimens after HCl etching are shown in Fig. 2a to d, respectively. The densities of the three specimens were >97%, so that only a few pores were observed after sintering. After HCl etching for 80 h, the In_2O_3 phase has been removed completely. Therefore, in Fig. 2b to 2d, solids correspond to the cubic-ZrO_2 phase, and pores correspond to the removed cubic-In_2O_3 phase. Grain and pore sizes were less than 1 μm. One can find that both the cubic-ZrO_2 and the cubic-In_2O_3 phases form 3D networks. Therefore these two-phase materials are 3D submicron size composites consisting of the continuous oxygen-ion-conducting cubic-ZrO_2 phase, and the continuous electron-conducting cubic-In_2O_3 phase. The abrupt increase in electrical conductivity of compositions with $InO_{1.5}$ concentrations higher than 45 m/o was caused by the 3D connection of the cubic-In_2O_3 phase with a high electronic conductivity. The homogeneous distribution of the cubic-ZrO_2 grains and the cubic-In_2O_3

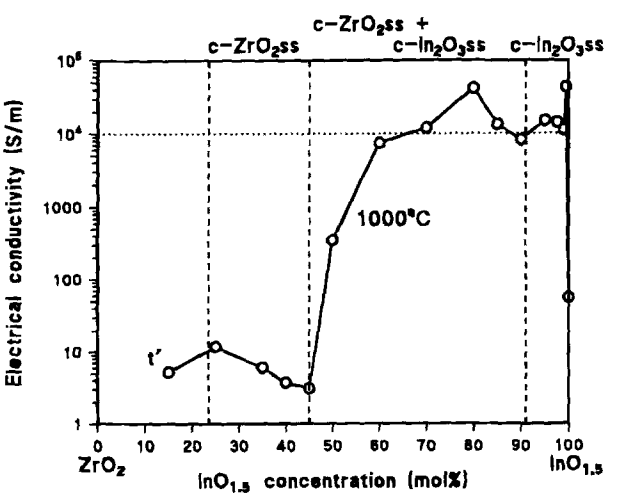

Fig. 1. Electrical conductivity of the In_2O_3-ZrO_2 system as a function of $InO_{1.5}$ concentration. The electrical conductivities in the ZrO_2-rich side of the system are taken from Ref. 2 and 9. The phase boundaries after sintering at 1500°C for 1 h are shown by dashed lines.

[a] Impurities detected by optical emission spectroscopy: Sn 8, Tl 4, Pb 2, Ni, Cu, Zn, Ag, Cd, Bi < 1 in ppm.

Downloaded on 2014-03-27 to IP 140.120.135.222 address. Redistribution subject to ECS terms of use (see ecsdl.org/site/terms_use) unless CC License in place (see abstract).

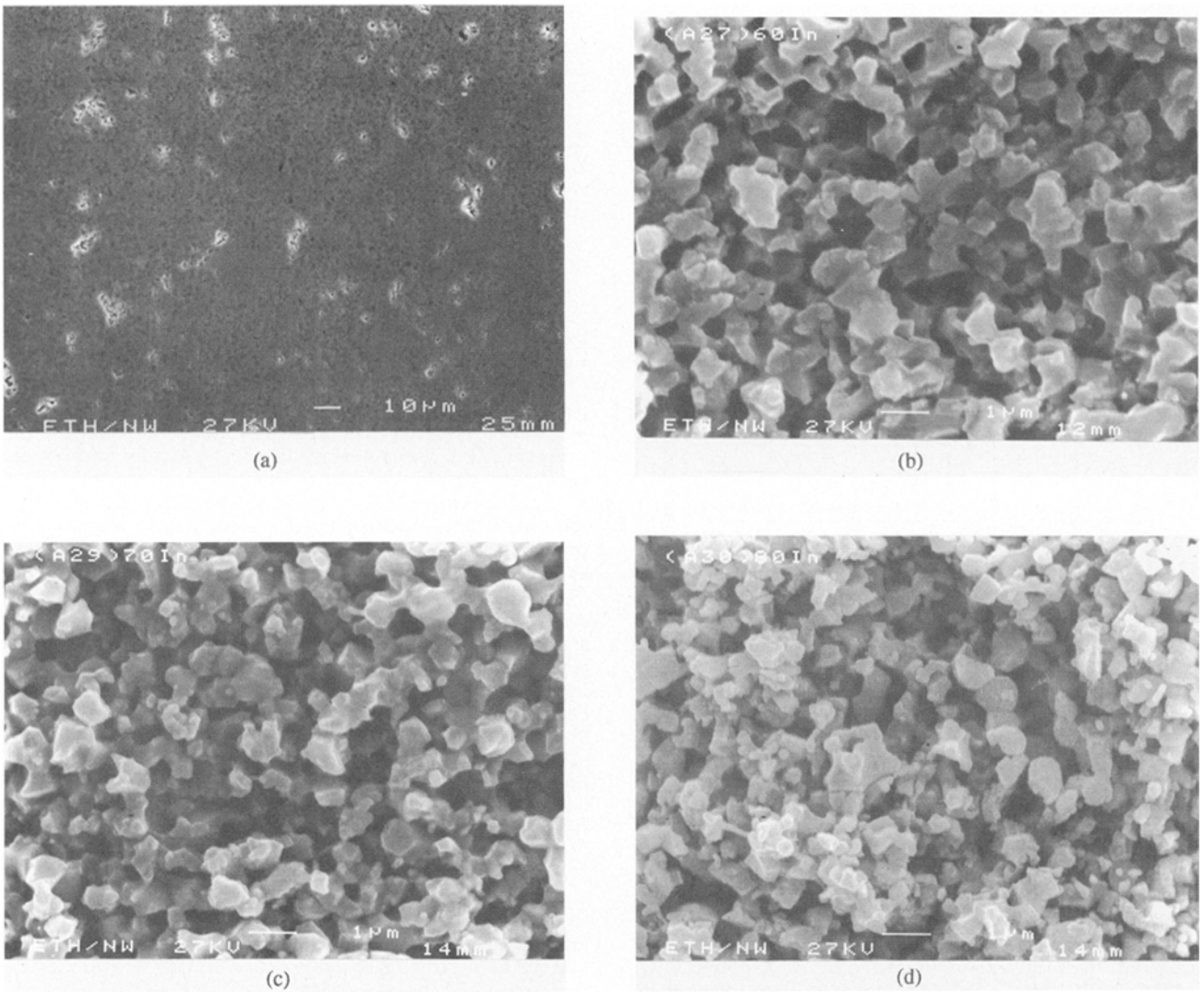

Fig. 2. SEM microstructure of (a) 80 m/o $InO_{1.5}$-ZrO_2 before HCl etching; and that of (b) 60 m/o; (c) 70 m/o; and (d) 80 m/o $InO_{1.5}$-ZrO_2 after HCl etching for 80 h. Note that the density of this specimen was more than 97% of theoretical and few pores were observed before HCl etching as shown in (a). Note the magnification difference.

grains was tailored using the coprecipitated In_2O_3-ZrO_2 powders, in which all ZrO_2 was metastably dissolved in the In_2O_3 crystallites of 30 nm diam after calcination at 800°C.[2,39] During sintering up to 1500°C, the cubic-ZrO_2 phase segregated from the cubic-In_2O_3 grains, forming the two-phase composites, in case the ZrO_2 concentration was much higher than 8 m/o.[2]

Electrical conductivity of In_2O_3 doped with ZrO_2.—Dopant concentration dependence.—The electrical conductivity of In_2O_3 doped with ZrO_2 was measured as a function of dopant concentration, temperature, and oxygen partial pressures. Figure 3 shows the electrical conductivity of In_2O_3-ZrO_2 as a function of $InO_{1.5}$ concentration >90 m/o, at 1250, 1100, and 1000°C. The doping with ZrO_2 enhanced the electrical conductivity of electronic character. The highest electrical conductivity in air was found in In_2O_3 doped with 0.5 m/o ZrO_2 (99.5 m/o $InO_{1.5}$), near the thermodynamic solubility limit of 0.6 m/o, according to the phase diagram of this system.[1,2]

The starting powders of In_2O_3-ZrO_2 were prepared via coprecipitation to achieve an initial homogeneous distribution of the elements. After this coprecipitation-and-calcination process, more ZrO_2 could be metastably dissolved in the cubic-In_2O_3 lattice, than under equilibrium conditions at high temperatures. After the calcination of the hydroxide precipitates, more than 40 m/o ZrO_2 could be retained in the cubic-In_2O_3.[1,2] Even after sintering at 1500°C for 1 h, 8 m/o ZrO_2 was dissolved metastably in the cubic-In_2O_3, indicating that the kinetics of phase separation are very sluggish. Due to this sluggish phase separation, the thermodynamic equilibrium in In_2O_3 could be achieved only if the specimens were heat-treated for more than 12 h even at 1500°C.[1,2] Figure 3 shows that in the ZrO_2-supersaturated single-phase region and above 1000°C the electrical conductivity decreased with decreasing $InO_{1.5}$ concentration (*i.e.*, with increasing ZrO_2 concentration from 0.5 to 10 m/o). A minimum was found at 90 m/o $InO_{1.5}$, near the metastable solubility limit after sintering at 1500°C for 1 h. Further increase in ZrO_2 concentration led to an increase in electrical conductivity to reach a maximum at 80 m/o $InO_{1.5}$-ZrO_2, as shown in Fig. 1.

Temperature dependence.—Figure 4 shows the temperature dependence of electrical conductivities of 80, 95, 99.5 m/o $InO_{1.5}$-ZrO_2 and pure In_2O_3. The electrical conductivities were measured on cooling from 1300°C to room temperature. The electrical conductivity of pure In_2O_3 decreased slightly with increasing temperature up to 800°C. Above 800°C, the electrical conductivity increased with increasing temperature. The electrical conductivity of doped-In_2O_3 was at least 2 orders of magnitude higher than that of pure In_2O_3 in the whole temperature range between 1300°C and room temperature. Therefore, the electrical conductivity of the doped-In_2O_3 is extrinsic, and is introduced by doping with ZrO_2.

The electrical conductivities of 80 and 99.5 m/o $InO_{1.5}$ exhibited the same temperature dependence. The conduc-

Downloaded on 2014-03-27 to IP 140.120.135.222 address. Redistribution subject to ECS terms of use (see ecsdl.org/site/terms_use) unless CC License in place (see abstract).

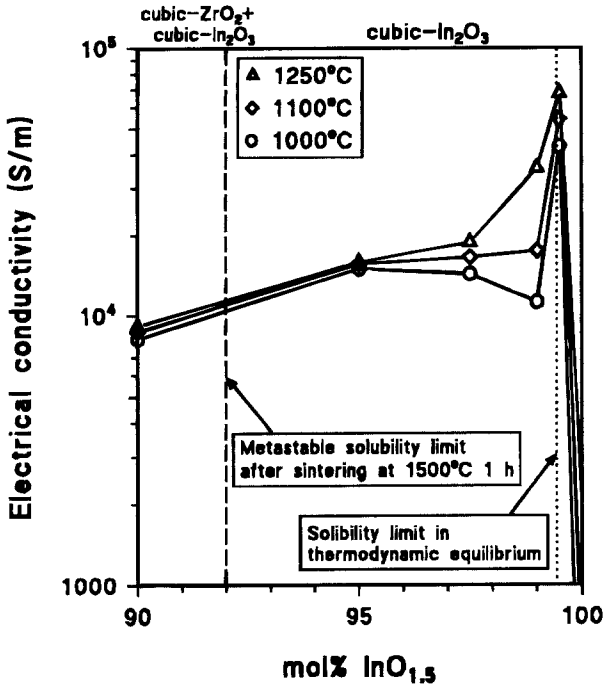

Fig. 3. Electrical conductivity of ZrO_2-$InO_{1.5}$ with $InO_{1.5}$ concentrations above 90 m/o, at 1250, 1100, and 1000°C.

tivities were almost independent of temperature from room temperature to 600°C, increased above 600°C with increasing temperature, and became less dependent on temperature around 1300°C. The electrical conductivity of 95 m/o $InO_{1.5}$ remained constant in the whole temperature range.

Oxygen partial pressure dependence.—The specimens of 80, 95, 97.5, 99.5 m/o $InO_{1.5}$-ZrO_2 and pure In_2O_3 were selected to measure the p_{O_2} dependence of electrical conductivity. Figure 5 shows electrical conductivities of (a) pure In_2O_3 at 1300, 1150, and 1000°C, and (b) ZrO_2-doped In_2O_3 at 1300 and 1000°C. The slopes of $\log \sigma$ *vs.* $\log p_{O_2}$ are calculated and compiled in Table I. In a reducing atmosphere, the doped-In_2O_3 exhibited higher electrical conductivity than in air. At the oxygen partial pressure of 5×10^{-5} atm, the highest electrical conductivity of 1.1×10^5 Sm^{-1} was found in 80 m/o $InO_{1.5}$-ZrO_2 at 1300°C.

Pure In_2O_3 possessed a p_{O_2} dependence of the exact $-1/6$ power law, in a reducing atmosphere of the p_{O_2} range from 5×10^{-5} to 0.01 atm. In the p_{O_2} range above 0.01, the conductivity became less dependent on p_{O_2}. In 80, 97.5, and

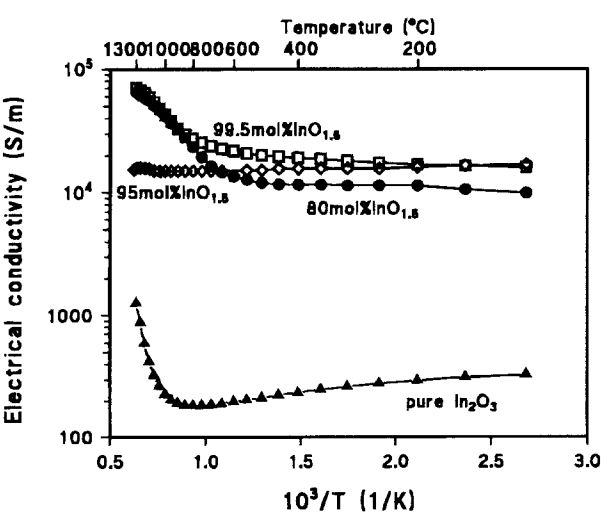

Fig. 4. The temperature dependence of the electrical conductivity of pure In_2O_3, and 80, 95, and 99.5 m/o $InO_{1.5}$-ZrO_2, measured from 1300°C to room temperature.

99.5 m/o $InO_{1.5}$-ZrO_2, a p_{O_2} dependence of the $-1/8$ power law was found, in the p_{O_2} range between 0.21 and 1 atm at 1000°C. However, with increasing temperature from 1000 to 1300°C, and/or with decreasing p_{O_2} below 0.21, the conductivity became less dependent on p_{O_2}. In 95 m/o $InO_{1.5}$-ZrO_2, the conductivity was independent of p_{O_2} at 1000°C. With increasing temperature from 1000 to 1300°C, however, it exhibited a p_{O_2} dependence, contrary to the 80 and 99.5 $InO_{1.5}$-ZrO_2 samples.

Electrical conductivity of In_2O_3 doped with various oxides.—Besides In_2O_3-ZrO_2 materials, In_2O_3 powders doped with SnO_2, CeO_2, Nb_2O_5, Pr_6O_{11}, as well as MgO were prepared via the coprecipitation process, with cation concentrations of 5 and 20 m/o. Table II shows the phase compositions of the powders after calcination at 800°C for 1 h, and those after sintering at 1500°C for 1 h. The metastable supersaturation of dopants in starting powders frequently was observed after the coprecipitation-and-calcination process. After the sintering, the 5 m/o oxide containing specimens with SnO_2, Nb_2O_5, Pr_6O_{11} as well as ZrO_2 consisted of the cubic-In_2O_3 phase only. The sintered specimens with CeO_2 and MgO included a small amount of second phases. After 20 m/o oxide addition, all sintered specimens, except that with SnO_2, were two-phase materials.

In Fig. 6, the electrical conductivities of In_2O_3 with (a) 5 and (b) 20 m/o addition of these oxides are shown. The additions of SnO_2, ZrO_2, Nb_2O_5, and CeO_2 increased the electrical conductivity. In the 5 m/o addition, ZrO_2-doped In_2O_3, even supersaturated in ZrO_2, exhibited an electrical conductivity comparable to SnO_2-doped In_2O_3. Among the 20 m/o added materials, the ZrO_2-containing specimen exhibited the highest electrical conductivity above 600°C. A high concentration of acceptor cations, such as MgO, led to a highly resistive n-type conductor.[46] ZrO_2 is a most effective donor for increasing electronic conductivity of In_2O_3.

Discussion

Lattice defect reactions in pure and doped In_2O_3.—Lattice defect reactions taken into account are compiled in Table III.[2,38,48-51] The specific p_{O_2} regions I, II, III, and IV are defined as p_{O_2} (region I) < p_{O_2} (region II) < p_{O_2} (region III) < p_{O_2} (region IV). The subscripts D and A indicate the tetravalent metal oxide (donor) doping and the divalent metal oxide (acceptor) doping, respectively. The regions III_D, III'_D, III''_D, and III'''_D are specified by the degree of defect association. The p_{O_2} dependences of electronic conductivity are derived for each defect mechanism based on the mass-action, mass-conservation, and electroneutrality conditions as described in Table III. According to the earlier studies,[49,51] the direct band-to-band transition mechanism and the mechanisms involving cation vacancies and cation interstitials are excluded as predominant mechanisms for electronic conduction in further discussion.

In the simple nonassociated defect model, where two ionic defects (oxygen vacancies and oxygen interstitials) and two electronic defects (electrons and holes) are involved, the lattice defect reactions in In_2O_3 may be described based on the following three primary reactions[19,37]

$$O_O^{\times} \overset{K_V}{\longleftrightarrow} V_O^{\bullet\bullet} + 2e' + 1/2\ O_2(g) \qquad [2]$$

$$O_O^{\times} \overset{K_F}{\longleftrightarrow} V_O^{\bullet\bullet} + O_i'' \qquad [3]$$

$$\text{null} \overset{K_B}{\longleftrightarrow} e' + h^{\bullet} \qquad [4]$$

The model can be expanded to include defect association reactions such as

$$(2Zr_{In}^{\bullet\bullet} \cdot O_i'')^{\times} \overset{K_A}{\longleftrightarrow} 2Zr_{In}^{\bullet} + O_i'' \qquad [5]$$

The relations among the equilibrium concentrations of defects are obtained with equilibrium constants defined as[19,35]

$$K_V = [V_O^{\bullet\bullet}] \cdot n^2 \cdot p_{O_2}^{1/2} = K_V^0 \cdot \exp(-\Delta E_V/kT) \qquad [6]$$

$$K_F = [V_O^{\bullet\bullet}] \cdot [O_i''] = K_F^0 \cdot \exp(-\Delta E_F/kT) \qquad [7]$$

Downloaded on 2014-03-27 to IP 140.120.135.222 address. Redistribution subject to ECS terms of use (see ecsdl.org/site/terms_use) unless CC License in place (see abstract).

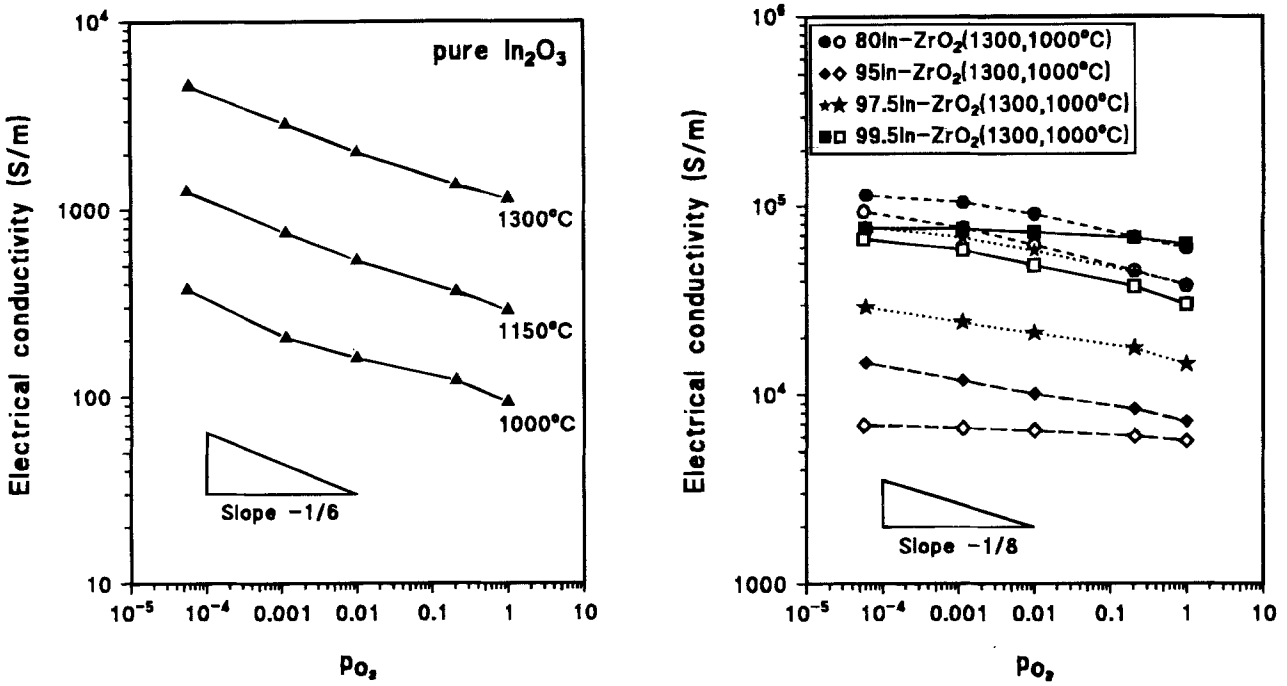

Fig. 5. The oxygen partial pressure dependence of the electrical conductivity of (a, left) pure In_2O_3, at 1300, 1150, and 1000°C, and (b, right) 80, 95, 97.5, and 99.5 m/o $InO_{1.5}$-ZrO_2, at 1300 and 1000°C.

$$K_B = n \cdot p = N_C \cdot N_v \cdot \exp(-\Delta E_B/kT) \quad [8]$$

$$K_A = [(2Zr_{In}^{\bullet} \cdot O_i'')^{\times}]^{-1} \cdot [Zr_{In}^{\bullet}]^2 \cdot [O_i''] = K_A^0 \cdot \exp(-\Delta E_A/kT) \quad [9]$$

where ΔE_V, ΔE_F, and ΔE_B are the formation energies of an ionized oxygen vacancy and two free-electrons by partial reduction, an oxygen Frenkel pair and an electron-hole pair, (bandgap), respectively, and ΔE_A is the dissociation energy of the $(2Zr_{In}^{\bullet} \cdot O_i'')^{\times}$ associate.

Neglecting the cation vacancies and cation interstitials, the overall electroneutrality condition is given by

$$[Zr_{In}^{\bullet}] + 2[V_O^{\bullet\bullet}] + p = 2[O_i''] + n \quad [10]$$

For most conditions of doping, temperature, and oxygen partial pressure, one positively charged species and one negatively charged species predominate,[35] and the overall electroneutrality condition can be simplified in specific conditions.

In models involving defect association reactions, the conservation condition of the total concentration of zirconium arises such as

$$c_{ZrO_2} = [Zr_{In}^{\bullet}] + 2[(2Zr_{In}^{\bullet} \cdot O_i'')^{\times}] \quad [11]$$

In considerably reducing atmosphere or in pure In_2O_3 (region I), the overall electroneutrality condition is reduced to $2[V_O^{\bullet\bullet}] = n$ and the other defects are negligible. The total defect reaction can be described as

$$In_2O_3 \leftrightarrow 2In_{In}^{\times} + 3V_O^{\bullet\bullet} + 6e' + 3/2\ O_2(g) \quad [12]$$

The electroneutrality condition and Eq. 6 yield

$$\sigma_e \propto n = (2K_V^0)^{1/3} \cdot \exp(-\Delta E_V/3kT) \cdot p_{O_2}^{-1/6} \quad [13]$$

The electronic conductivity depends on $p_{O_2}^{-1/6}$ due to the partial reduction of In_2O_3 forming oxygen vacancies and free-electrons, under the condition that the mobility of electrons remains constant.

In_2O_3 possesses the C-type rare-earth structure, which is tolerant for retaining oxygen vacancies or oxygen interstitials as mentioned in the beginning of the paper. If ZrO_2 is dissolved in the In_2O_3 lattice, oxygen interstitials could be introduced to maintain charge neutrality. At atmospheric oxygen partial pressure, oxygen interstitials are responsible for oxygen diffusion in In_2O_3 with 1 m/o ZrO_2 as an impurity.[19] The oxygen interstitial formation was confirmed in SnO_2-doped In_2O_3.[38] In ZrO_2-doped In_2O_3, the total defect reaction may be described as

$$2ZrO_2 \xrightarrow{In_2O_3} 2Zr_{In}^{\bullet} + 3\ O_O^{\times} + O_i''$$

$$O_i'' \leftrightarrow 2e' + 1/2\ O_2(g) \quad [14]$$

In moderately reducing conditions (region II_D), where $n >> 2[O_i'']$, most of oxygen interstitials are reduced leaving electrons. The electroneutrality condition is $[Zr_{In}^{\bullet}] = n$. The total defect reaction 14 can be simplified to

$$2ZrO_2 \xrightarrow{In_2O_3} 2Zr_{In}^{\bullet} + 3\ O_O^{\times} + 2e' + 1/2\ O_2(g) \quad [15]$$

In the nonassociated case, the electronic conductivity can be described as

$$\sigma_e \propto n = [Zr_{In}^{\bullet}] \approx c_{ZrO_2} \quad [16]$$

The electronic conductivity remains constant with temperature and oxygen partial pressure. The free (mobile) electron concentration is identical to the doped ZrO_2 concentration.

In oxidizing atmosphere (region III_D), where $2[O_i''] >> n$, the electronic conductivity may be attributed to the reduction of isolated oxygen interstitials. The overall electroneutrality condition is simplified to $[Zr_{In}^{\bullet}] = 2[O_i'']$. In In_2O_3 doped with a hypervalent metal oxide, the oxygen vacancy concentration is much lower than the oxygen interstitial concentration, as expected from Eq. 3 and 14. The electroneutrality condition and Eq. 6 and 7 yield

$$\sigma_e \propto n = (K_V^0/K_F^0)^{1/2} \cdot ([Zr_{In}^{\bullet}]/2)^{1/2} \cdot \exp(-(\Delta E_V - \Delta E_F)/2kT) \cdot p_{O_2}^{-1/4} \quad [17]$$

where $[Zr_{In}^{\bullet}] = c_{ZrO_2}$ in the nonassociated case. The electronic conductivity exhibits the p_{O_2} dependence of the $-1/4$ power law.

If the defect association is not negligible (region III_D''), the defect reactions involving reaction 5 are described as

$$2ZrO_2 \xrightarrow{In_2O_3} (2Zr_{In}^{\bullet} \cdot O_i'')^{\times} + 3\ O_O^{\times}$$

$$(2Zr_{In}^{\bullet} \cdot O_i'')^{\times} \leftrightarrow 2Zr_{In}^{\bullet} + 2e' + 1/2\ O_2(g) \quad [18]$$

Downloaded on 2014-03-27 to IP 140.120.135.222 address. Redistribution subject to ECS terms of use (see ecsdl.org/site/terms_use) unless CC License in place (see abstract).

Table I. Oxygen partial pressure dependence of electrical conductivity of pure and ZrO_2-doped In_2O_3.

Temperature (°C)	p_{O_2} range (atm)	p_{O_2} dependence (Slope log σ *vs.* log p_{O_2}) 80 m/o $InO_{1.5}$-20%ZrO_2 (two phase)	95 m/o $InO_{1.5}$-5% ZrO_2 (supersaturated)	97.5 m/o $InO_{1.5}$-2.5% ZrO_2 (single phase)	99.5 m/o $InO_{1.5}$-0.5% ZrO_2 (single phase)	Pure In_2O_3
1300	0.21-1	−1/11.3	−1/10.1	−1/10.4	−1/21	−1/9.1
	5×10^{-5} − 0.21	−1/15.8	−1/14.5	−1/14.5	−1/67	−1/6.7
	(5×10^{-5} − 0.01)					(−1/6.4)
1150	0.21-1	—	—	—	—	−1/6.8
	5×10^{-5} − 0.21	—	—	—	—	−1/6.6
	(5×10^{-5} − 0.01)					(−1/6.0)
1000	0.21-1	−1/8.5	−1/24	−1/7.9	−1/7.7	−1/6.0
	5×10^{-5} − 0.21	−1/11.3	−1/65	−1/16.4	−1/13.7	−1/7.4
	(5×10^{-5} − 0.01)					(−1/6.0)

Table II. Phase composition after calcination and sintering of In_2O_3 doped with various oxides.

	After calcination at 800°C for 1 h		After sintering at 1500°C for 1 h	
	95 m/o $InO_{1.5}$-5% MO_x	80 m/o $InO_{1.5}$-20% MO_x	95 m/o $InO_{1.5}$-5% MO_x	80 m/o $InO_{1.5}$-20% MO_x
ZrO_2	bcc-In_2O_3	bcc-In_2O_3	bcc-In_2O_3	bcc-In_2O_3 + fcc-ZrO_2
SnO_2	bcc-In_2O_3	bcc-In_2O_3	bcc-In_2O_3	bcc-In_2O_3
CeO_2	bcc-In_2O_3 + fcc-CeO_2	bcc-In_2O_3 + fcc-CeO_2	bcc-In_2O_3 + fcc-CeO_2	bcc-In_2O_3 + fcc-CeO_2
Nb_2O_5	bcc-In_2O_3	bcc-In_2O_3 + m-$InNbO_4$	bcc-In_2O_3	bcc-In_2O_3 + m-$InNbO_4$
Pr_6O_{11}	bcc-In_2O_3	bcc-In_2O_3	bcc-In_2O_3	bcc-In_2O_3 + o-$PrInO_3$
MgO	bcc-In_2O_3	bcc-In_2O_3	bcc-In_2O_3 + fcc-In_2MgO_4	bcc-In_2O_3 + fcc-In_2MgO_4

The mass conservation condition of zirconium (Eq. 11) and the defect association reaction (Eq. 5) should be taken into account also. In the fully associated case $2[(2Zr_{In}^{\bullet} \cdot O_i'')^{\times}] >> [Zr_{In}^{\bullet}]$, Eq. 11 is reduced to $c_{ZrO_2} \approx 2[(2Zr_{In}^{\bullet} \cdot O_i'')^{\times}]$. This mass-conservation condition, the electroneutrality condition $[Zr_{In}^{\bullet}] \approx n$ expected from Eq. 18, and the Eq. 6, 7, and 9 give

$$\sigma_e \propto n = (K_V^0 \cdot K_A^0/K_F^0)^{1/4} \cdot (c_{ZrO_2}/2)^{1/4} \cdot \exp(-(\Delta E_V - \Delta E_F + \Delta E_A)/4kT) \cdot p_{O_2}^{-1/8} \quad [19]$$

Therefore the electronic conductivity exhibits a −1/8 power dependence on p_{O_2} under the condition that the mobility remains constant. With decreasing oxygen partial pressure, the oxygen interstitials in the neutral associates are reduced and the electron concentration becomes $n \approx c_{ZrO_2}$, as in the moderately reducing condition mentioned before (region II_D).

The law of mass action may not be valid in heavily doped materials (region III_D''), when the dopant concentration is much higher than 1 m/o.[52,53] In highly SnO_2-doped In_2O_3 films, the electronic conductivity and the electron mobility decrease due to the formation of associated defect complexes,[38] and the tin donor ions become neutralized forming SnO_2 or Sn_3O_4 clusters in In_2O_3 grains.[20,26,54,55] One example of possible defect associations in ZrO_2-doped In_2O_3 is shown in Table III.

Electronic conduction mechanisms.—Pure In_2O_3.—The slope of −1/6 in the log σ *vs.* log p_{O_2} plot was observed in the reducing atmosphere in the pure In_2O_3. This p_{O_2} dependence corresponds to the partial reduction of In_2O_3 forming oxygen vacancies, consistent with the earlier studies.[48,49] The mechanisms with oxygen interstitials and indium vacancies are excluded in pure In_2O_3, since they should cause a positive p_{O_2} dependence, as described in Table III. The mechanism with indium interstitial may be excluded because the p_{O_2} dependence of the −3/16 power law was not observed, consistent with the earlier studies.[48,49]

The electrical conductivity of electronic character increased with increasing temperature above 800°C. The p_{O_2} dependence study has revealed that the electronic conductivity is determined by the partial reduction of In_2O_3 at 1000 and 1300°C. Using the electrical conductivity data at and below 0.01 atm in Fig. 5a, the activation energy defined by $\sigma = \sigma_0 \cdot \exp(-\Delta E/kT)$ was calculated to be $\Delta E = 1.47 \pm 0.03$ eV, consistent with that of the earlier studies.[51,56] Consequently, the activation energy of this defect reaction defined by Eq. 5 was calculated to be $\Delta E_V = 4.41$ eV above 1000°C.

Below 800°C, the pure In_2O_3 exhibited a conductivity of metallic character, that is, the electronic conductivity decreases gradually with increasing temperature. This metallic behavior has been observed previously in pure In_2O_3.[51,57] The electrical conductivities in Fig. 3 and 4 were measured on cooling at a rate of 4°C/min. At lower temperatures, a high temperature state is frozen and the electrical conductivity data are not necessarily the same as those in equilibrium. The electrical conductivity data measured on cooling differed from those in equilibrium even at 1000°C in 95 m/o $In_{1.5}$-ZrO_2 and pure In_2O_3, shown in Fig. 5a and b.[b] At far lower temperatures, little change in electrical conductivity was observed by varying oxygen partial pressure, indicating that no exchange of oxygen occurred between the specimens and the atmosphere. In this situation, the electronic conductivity may be determined by the mobility change (metallic) or the activation of donors (semiconducting) rather than the defect equilibria with the atmosphere.

Single-phase region.—Since the electrical conductivity is extrinsic in ZrO_2-doped In_2O_3, the increased electrical conductivity in doped specimens cannot be explained by the partial reduction of In_2O_3. Further, the doping of In_2O_3 with hypervalent metal oxides should depress the oxygen vacancy concentration in In_2O_3, as expected from Eq. 14. Therefore, the free-electron concentration introduced by the partial reduction should be decreased by doping with ZrO_2, which results in a decrease in electronic conductivity, contrary to the experimental results. To elucidate possible defect models, the oxygen partial pressure dependence of the electronic conductivity should be examined.

The slope of −1/8 in the log σ *vs.* log p_{O_2} plot was found in 80, 97.5, and 99.5 m/o $InO_{1.5}$-ZrO_2 in the oxidizing atmosphere at 1000°C. This p_{O_2} dependence corresponds to the mechanism with oxygen interstitial-dopant cation (neutral) pairs, as described in the previous Section as well as in Table III. The slopes were −1/8.5, −1/7.9, and −1/7.7 in the 80, 97.5, and 99.5 m/o $InO_{1.5}$ specimens, respectively, at 1000°C in the p_{O_2} range between 0.21 and 1 atm, as shown in Table I. With decreasing p_{O_2} to 5×10^{-5} and/or with

[b] For both specimens, much longer time (>24 h) was needed for equilibration, suggesting slow oxygen diffusion kinetics compared with those in the 80, 97.5, and 99.5 m/o specimens. The oxygen vacancy concentration is very low in the oxidizing atmosphere in pure In_2O_3, and the oxygen interstitials may be tightly bound forming complexes in the heavily doped 95 m/o $InO_{1.5}$-ZrO_2, as mentioned later, both leading to low oxygen diffusivity.

Downloaded on 2014-03-27 to IP 140.120.135.222 address. Redistribution subject to ECS terms of use (see ecsdl.org/site/terms_use) unless CC License in place (see abstract).

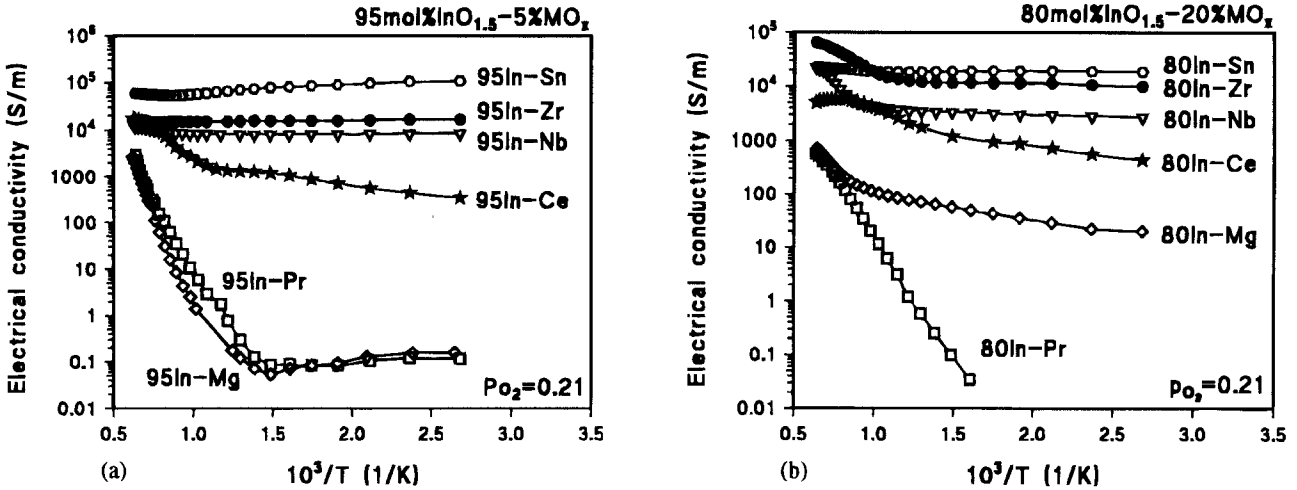

Fig. 6. Electrical conductivity of In_2O_3 with (a) 5 and (b) 20 cation m/o of metal oxides, ZrO_2, SnO_2, $NbO_{2.5}$, CeO_2, Pr_6O_{11}, as well as MgO.

increasing temperature up to 1300°C, the electrical conductivity became less dependent on p_{O_2} than the $-1/8$ power law, as shown in Fig. 5b. This transition can be explained assuming a transition occurs from the oxygen interstitial-dopant cation pair mechanism to the simple donor doping mechanism, where oxygen interstitials become reduced and the doped-In_2O_3 loses oxygen. The decrease in weight of In_2O_3 due to oxygen loss has been observed with increasing temperature above 900°C.[56]

The conclusion, that the transition occurs from the oxygen interstitial-dopant cation pair mechanism at 1000°C to the simple donor doping mechanism at 1300°C in the oxidizing atmosphere, is consistent with the temperature dependence of the both samples in Fig. 4. The conductivity became less dependent on temperature around 1300°C with increasing temperature. Both p_{O_2} and temperature dependences indicate that the equilibrium of the reversible reaction of Eq. 18 shifts to the right side either exponentially with increasing temperature or by the $-1/8$ power dependence with decreasing oxygen partial pressure, expected from Eq. 19.

The p_{O_2} dependence of the $-1/4$ power law was not observed in ZrO_2-doped In_2O_3 under our experimental conditions. This dependence is related to the reduction of isolated oxygen interstitials or singly charged oxygen interstitial-dopant cation pair, as described in Table III. However, these mechanisms may not be excluded especially when the dopant concentration is very low. If this mechanism is predominate, the slope of log σ *vs.* log p_{O_2} changes gradually from $-1/4$ to zero with decreasing oxygen partial pressure.

Based on the discussion above and the following calculations, the Kröger-Vink diagram (defect concentrations as a function of oxygen partial pressure) of 99.5 m/o $InO_{1.5}$-ZrO_2 can be constructed, as shown in Fig. 7. Assuming that the doped Zr^{4+} ions in this specimen are fully activated giving one electron per one Zr^{4+} ion at 1300°C and 5×10^{-5} atm, the free-electron concentration in this 0.5 m/o doped specimen was calculated to be 7.7×10^{25} m^{-3}, using the lattice constant of 1.0126 nm.[1,2] Since the electrical conductivity of n-type electronic character was 8×10^4 Sm^{-1} at the temperature and the p_{O_2}, the mobility of electrons, $\mu = \sigma/e \cdot n$, was derived to be 6.5×10^{-3} m^2 V^{-1} s^{-1}, comparable to that in slightly SnO_2-doped In_2O_3.[38] Using this mobility value and assuming that the mobility remains unchanged by doping if the dopant concentration is very low (0.5 m/o in this specimen), the electron concentration in pure In_2O_3 at 1000°C, was calculated from the conductivity data to be log n = 22.84 − 0.165 log p_{O_2} (m^{-3}). The equilibrium constant, defined by Eq. 6, was calculated to be $K_V = [V_O^{\bullet\bullet}] \cdot n^2 \cdot p_{O_2}^{1/2} \approx 1/2\, n^3 \cdot P_{O_2}^{1/2} = 10^{68.2}$ m^{-9}.

The extrapolation of the electronic conductivity data of 99.5 m/o $InO_{1.5}$-ZrO_2 in the oxidizing atmosphere showing the $-1/8$ power p_{O_2} dependence, to 8×10^4 Sm^{-1} yields the p_{O_2} boundary of 1.5×10^{-3} atm between the region II (simple donor doping mechanism) and the region III (oxygen interstitial-dopant cation pair mechanism). In the same way, the extrapolation of the electronic conductivity data of pure In_2O_3 at 1000°C to 8×10^4 Sm^{-1} results in a p_{O_2} boundary of 5×10^{-19} atm, below which the partial reduction of In_2O_3 is predominate (region I).

The equilibrium constant K_B, the product of the electron and hole concentrations, was calculated[58] to be $K_B = 10^{44.3}$ m^{-6} at 1000°C. The bandgap for indirect transition of 2.62 eV [60,61] at room temperature, the temperature coefficient of the bandgap $\beta = 1.0 \times 10^{-3}$ eV/K,[60] the effective mass of $m_c^* = 0.35$ m[14,38] and $m_v^* = 0.7$ m[62] were used for the calculation. For the simplicity, K_B is defined based on the classical mass action law and the Maxwell-Boltzmann statistics for nondegenerated semiconductors, as described in Eq. 8. In doped In_2O_3 with a higher electron concentration, this classical treatment with an equilibrium constant K_B may become invalid and the doped In_2O_3 should be treated as a degenerated semiconductor.[19,58] The slopes of log [Defect] *vs.* log p_{O_2} for each defect species were derived using the mass action law and the electroneutrality and mass-conservation conditions described in the previous Section as well as in Table III. Consequently, the Kröger-Vink diagram of 99.5 m/o $InO_{1.5}$-ZrO_2 can be constructed as shown in Fig. 7, including the defect associate $(2Zr_{In}^{\bullet} \cdot O_i'')^{\times}$. In the nonassociated case, the concentration of electrons and holes may exhibit the $-1/4$ dependence instead of the $-1/8$ dependence in the region III, and $[O_i'']$ instead of $[(2Zr_{In}^{\bullet} \cdot O_i'')^{\times}]$ is the predominate defect species. The stability of the cubic In_2O_3 phase is not taken into account in this diagram. The sublimation of In_2O_3 [56,63] and the transformation to the hexagonal phase[64] occurs at extremely low and high oxygen partial pressures, respectively.

This diagram suggests that the dopant is not always fully activated, producing two free-electrons. Oxygen interstitials are involved in the defect equilibria as $c_{MO_2} = 2[O_i''] + n$. At a high oxygen partial pressure, the hypervalent metal oxide doping is compensated by the formation of oxygen interstitials rather than by the formation of free-electrons. Further, even when the dopant concentration is very low, defect interactions may not be ignored and may influence the electronic conductivity.

Two-phase region.—The 80 m/o $InO_{1.5}$-ZrO_2 exhibited a similar dependence on both temperature and p_{O_2}, to the 99.5 m/o $InO_{1.5}$ material. This behavior can be explained if the equilibrium of the cation distribution has been achieved in 80 m/o $InO_{1.5}$-ZrO_2. In this case, the cubic-In_2O_3 grains contain 0.6 m/o ZrO_2, the ZrO_2 concentration at the solubility limit in equilibrium. 20 m/o ZrO_2 is far from the solubility limit in equilibrium, and the phase separation kinetics at 1500°C were fast enough to reach equilibrium. The 80 m/o specimen consists of the cubic-In_2O_3 and the

Downloaded on 2014-03-27 to IP 140.120.135.222 address. Redistribution subject to ECS terms of use (see ecsdl.org/site/terms_use) unless CC License in place (see abstract).

Table III. Lattice defect reactions and oxygen partial pressure dependence of electronic conductivity of pure and doped In_2O_3.

	Region	Defect reactions	Mass action law/ Mass-conservation condition	Electroneutrality condition	Electronic conductivity vs. Po_2	Ref.
Intrinsic	I	Oxygen vacancy formation $O_o^x \xleftrightarrow{K_V} V_o^{\cdot\cdot} + 2e' + \frac{1}{2}O_2$	$K_V = [V_o^{\cdot\cdot}] \cdot n^2 \cdot Po_2^{1/2}$	$2[V_o^{\cdot\cdot}] = n$	$\sigma \propto n = (2K_V)^{1/3} \cdot Po_2^{-1/6}$	48,49
	IV	Oxygen interstitial formation $O_2 \leftrightarrow 2O_i'' + 4h^{\cdot}$	$K_V = [V_o^{\cdot\cdot}] \cdot n^2 \cdot Po_2^{1/2}$ $K_F = [V_o^{\cdot\cdot}] \cdot [O_i'']$ $K_B = n \cdot p$	$p = 2[O_i'']$	$\sigma \propto p = \left(\frac{2K_F \cdot K_B^2}{K_V}\right)^{1/3} \cdot Po_2^{1/6}$	-----
	-----	Indium vacancy formation $\frac{1}{2}O_2 \xleftrightarrow{K_I} 2V_{In}''' + 6h^{\cdot} + 3O_o^x$	$K_I = [V_{In}''']^2 \cdot p^6 \cdot Po_2^{-1/2}$	$p = 3[V_{In}''']$	$\sigma \propto p = (9K_I)^{1/4} \cdot Po_2^{3/16}$	-----
	-----	Indium interstitial formation $In_2O_3 \xleftrightarrow{K_{II}} 2In_i^{\cdot\cdot\cdot} + 6e' + \frac{1}{2}O_2$	$K_{II} = [In_i^{\cdot\cdot\cdot}]^2 \cdot n^6 \cdot Po_2^{1/2}$	$3[In_i^{\cdot\cdot\cdot}] = n$	$\sigma \propto n = (9K_{II})^{1/4} \cdot Po_2^{-3/16}$	-----
	-----	Valence-conduction band transition $null \xleftrightarrow{K_B} e' + h^{\cdot}$	$K_B = n \cdot p$	$p = n$	$\sigma \propto n = K_B^{1/2} \neq f(Po_2)$ $(\sigma \propto exp(-\Delta E_B / 2kT))$	49,51
Extrinsic (MO_2 doping)	II_D	Simple donor doping $2MO_2 \xrightarrow{In_2O_3} 2M_{In}^{\cdot} + 3O_o^x + 2e' + \frac{1}{2}O_2$	-----	$[M_{In}^{\cdot}] = n$	$\sigma \propto n \neq f(Po_2)$	48
	III_D	Reduction of isolated oxygen interstitial $2MO_2 \xrightarrow{In_2O_3} 2M_{In}^{\cdot} + 3O_o^x + O_i''$ $O_i'' \leftrightarrow 2e' + \frac{1}{2}O_2$	$K_V = [V_o^{\cdot\cdot}] \cdot n^2 \cdot Po_2^{1/2}$ $K_F = [V_o^{\cdot\cdot}] \cdot [O_i'']$	$[M_{In}^{\cdot}] = 2[O_i'']$	$\sigma \propto n = \left(\frac{K_V \cdot [M_{In}^{\cdot}]}{2K_F}\right)^{1/2} \cdot Po_2^{-1/4}$	-----
	III_D'	Reduction of oxygen interstitial-dopant pair (singly-charged) $2MO_2 \xrightarrow{In_2O_3} (M_{In}^{\cdot} \cdot O_i'')' + M_{In}^{\cdot} + 3O_o^x$ $(M_{In}^{\cdot} \cdot O_i'')' \xleftrightarrow{K_A'} M_{In}^{\cdot} + O_i''$ $O_i'' \leftrightarrow 2e' + \frac{1}{2}O_2$	$K_V = [V_o^{\cdot\cdot}] \cdot n^2 \cdot Po_2^{1/2}$ $K_F = [V_o^{\cdot\cdot}] \cdot [O_i'']$ $K_A' = [(M_{In}^{\cdot} \cdot O_i'')']^{-1} \cdot [M_{In}^{\cdot}] \cdot [O_i'']$ $c_{MO_2} = [(M_{In}^{\cdot} \cdot O_i'')']$	$[M_{In}^{\cdot}] = [(M_{In}^{\cdot} \cdot O_i'')']$	$\sigma \propto n = \left(\frac{K_V \cdot K_A'}{K_F}\right)^{1/2} \cdot Po_2^{-1/4}$	-----
	III_D''	Reduction of oxygen interstitial-dopant pair (neutral) $2MO_2 \xrightarrow{In_2O_3} (2M_{In}^{\cdot} \cdot O_i'')^x + 3O_o^x$ $(2M_{In}^{\cdot} \cdot O_i'')^x \xleftrightarrow{K_A} 2M_{In}^{\cdot} + O_i''$ $O_i'' \leftrightarrow 2e' + \frac{1}{2}O_2$	$K_V = [V_o^{\cdot\cdot}] \cdot n^2 \cdot Po_2^{1/2}$ $K_F = [V_o^{\cdot\cdot}] \cdot [O_i'']$ $K_A = [(2M_{In}^{\cdot} \cdot O_i'')^x]^{-1} \cdot [M_{In}^{\cdot}]^2 \cdot [O_i'']$ $c_{MO_2} = 2[(2M_{In}^{\cdot} \cdot O_i'')^x]$	$[M_{In}^{\cdot}] = n$	$\sigma \propto n = \left(\frac{K_V \cdot K_A \cdot c_{MO_2}}{2K_F}\right)^{1/4} \cdot Po_2^{-1/6}$ $(\because [(2Zr_{In}^{\cdot} \cdot O_i'')^x] >> [O_i''])$	38
	III_D'''	Association of defect complexes $2MO_2 \xrightarrow{In_2O_3} (2M_{In}^{\cdot} \cdot O_i'')^x + 3O_o^x$ $2MO_2 \xrightarrow{In_2O_3} (M_2 \cdot O_4)^x$ $(2M_{In}^{\cdot} \cdot O_i'')^x + (M_2 \cdot O_4)^x$ $\leftrightarrow [(2M_{In}^{\cdot} \cdot O_i'')^x \cdot (M_2 \cdot O_4)^x]$	-----	-----	$\sigma \neq f(Po_2)$	38
Extrinsic (AO doping)	II_A	Oxidation of oxygen vacancy $2AO \xrightarrow{In_2O_3} 2A_{In}' + 2O_o^x + V_o^{\cdot\cdot}$ $V_o^{\cdot\cdot} + \frac{1}{2}O_2 \leftrightarrow O_o^x + 2h^{\cdot}$ $O_o^x \leftrightarrow V_o^{\cdot\cdot} + 2e' + \frac{1}{2}O_2$	$K_V = [V_o^{\cdot\cdot}] \cdot n^2 \cdot Po_2^{1/2}$ $K_B = n \cdot p$	$2[V_o^{\cdot\cdot}] = [A_{In}']$	If $\mu_h \approx \mu_e$, $\sigma \propto p = K_B \cdot \left(\frac{[A_{In}']}{2K_V}\right)^{1/2} \cdot Po_2^{1/4}$ If $\mu_h << \mu_e$, $\sigma \propto n = \left(\frac{2K_V}{[A_{In}']}\right)^{1/2} \cdot Po_2^{-1/4}$	48
	III_A	Simple acceptor doping $2AO + \frac{1}{2}O_2 \xrightarrow{In_2O_3} 2A_{In}' + 3O_o^x + 2h^{\cdot}$	-----	$p = [A_{In}']$	$\sigma \propto p \neq f(Po_2)$	-----

c: dopant concentration; MO_2:tetravalent metal oxide; AO:divalent metal oxide; μ: mobility; n=[e']; p=[h'],
Po_2(region I)<Po_2(region II)<Po_2(region III)<Po_2(region IV),
regions II_D, III_D, III_D', III_D'', III_D''' for tetravalent metal oxide doping, regions II_A, III_A for divalent metal oxide doping.
K_V, K_F, K_B, K_A, K_I, K_{II}: equilibrium constants defined for specific reactions, see text for details or each defect reaction.
Electroneutrality conditions simplified from the overall electroneutrality condition: $3[In_i^{\cdot\cdot\cdot}] + [M_{In}^{\cdot}] + 2[V_o^{\cdot\cdot}] + p = 3[V_{In}'''] + [A_{In}'] + 2[O_i''] + n$.

cubic-ZrO_2. The electrical conductivity is dominated by the electronic conductivity of the cubic-In_2O_3 phase. The electronic conductivity of 80 m/o $InO_{1.5}$-ZrO_2 exceeded that of 99.5 m/o $InO_{1.5}$-ZrO_2 in the reducing atmosphere, as shown in Fig. 5b. This result suggests that the ZrO_2 concentration in the cubic In_2O_3 phase in the 80 m/o $InO_{1.5}$ specimen is slightly higher than 0.5 m/o, consistent with the solubility of 0.6 m/o ZrO_2 in the phase diagram.[1,2]

Supersaturated single-phase region.—Contrary to the other ZrO_2-doped specimens, the 95 m/o $InO_{1.5}$-ZrO_2 was a single-phase material, however, supersaturated in ZrO_2. In this material sintered at 1500°C for 1 h, the electrical conductivity was independent of p_{O_2} at 1000°C, and independent of temperature in air. Two situations are possible: the simple donor-doping mechanism and the association of defect complexes mechanism. Both models could exhibit less dependence on p_{O_2} and temperature. However, with increasing temperature from 1000 to 1300°C, the electrical conductivity became more dependent on p_{O_2}, as shown in Fig. 5b. With increasing temperature, the slope of log σ *vs.*

Downloaded on 2014-03-27 to IP 140.120.135.222 address. Redistribution subject to ECS terms of use (see ecsdl.org/site/terms_use) unless CC License in place (see abstract).

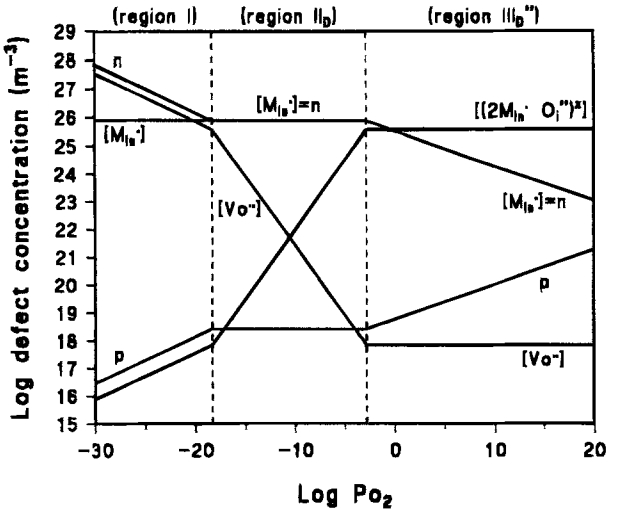

Fig. 7. The defect concentration in the 99.5 m/o $InO_{1.5}$-ZrO_2 solid solution as a function of oxygen partial pressure at 1000°C (Kröger-Vink diagram). M (tetravalent metal cation) = Zr^{4+}, substituted in the In_2O_3 cation sublattice. See Table III and the text for the definition of p_{O_2} regions.

log p_{O_2} changed from −1/24 to −1/10.1 in the oxidizing atmosphere, and from −1/65 to −1/14.5 in the reducing atmosphere, as shown in Table I. If the sample donor-doping mechanism is predominant and all Zr^{4+} ions are fully ionized as donors, the electrical conductivity becomes less dependent on p_{O_2} with increasing temperature. This is in contradiction to the experimental findings for this 95 m/o specimen. The experimental results can only be understood if one assumes that associated defect complexes at 1000°C decompose to simpler defect complexes such as oxygen interstitial-dopant cation pairs. These simple defect pairs yield the −1/8 power dependence on p_{O_2}. Therefore the conductivity in this ZrO_2-supersaturated material may be described by the association of defect complexes. This mechanism is predominant in heavily SnO_2-doped In_2O_3, when the SnO_2 concentration is higher than 4 m/o.[47] The transitions of electronic conduction mechanisms in the oxidizing atmosphere are described schematically in Fig. 8.

The slow phase separation kinetics give us an opportunity to make more hypervalent metal oxides, such as ZrO_2 and SnO_2, metastably doped in the In_2O_3 lattice. However the higher dopant concentration does not necessarily lead to a high electronic conductivity due to the defect complex formation. The tightly bound defect complexes in the supersaturated specimen are stable up to 1300°C in air, expected from the temperature independence of the electronic conductivity up to 1300°C, as shown in Fig. 4. The p_{O_2} dependences at 1000 and 1300°C in Fig. 5b indicate that both a high temperature and a reducing atmosphere are

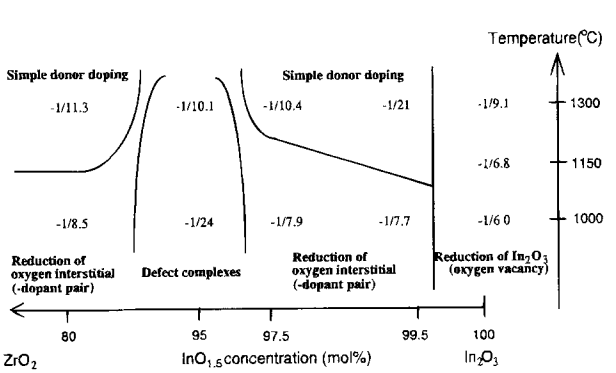

Fig. 8. Transition of electronic conduction mechanisms in In_2O_3 doped with ZrO_2. The slopes of log σ *vs.* log p_{O_2} in the oxidizing atmosphere (air to pure O_2) are also given.

needed for the bound oxygen interstitials to be reduced leaving free-electrons to obtain a high electronic conductivity. In heavy SnO_2 doping, the tin donor ions became neutralized forming SnO_2 or Sn_3O_4 clusters in In_2O_3 grains.[20,26,54,55] Further, the mobility may become lower with increasing dopant concentration due to the scattering of electron conduction by dopants and/or defect complexes as found in heavily SnO_2-doped In_2O_3.[16,38,65]

In the ZrO_2-supersaturated single-phase region, the electrical conductivity decreased with increasing ZrO_2 concentration, and a minimum was found at 90 m/o $InO_{1.5}$. The minimum was caused by the supersaturation, due to the slow segregation of ZrO_2 from the In_2O_3 grains. Therefore, we expect changes in conductivity with sintering time when these samples are kept at high temperatures. The electrical conductivity of 90 and 95 m/o $InO_{1.5}$-ZrO_2 at 1250°C increased from 1.0×10^4 to 3.8×10^4 Sm^{-1}, and from 1.5×10^4 to 7.3×10^4 Sm^{-1}, respectively, with increasing sintering time from 1 to 12 h. After 36 h sintering of the 90 m/o specimen at 1500°C, the electrical conductivities of 80, 90, 95, and 99.5 m/o $InO_{1.5}$ specimens were identical. This can be expected as the material becomes a two-phase mixture of the cubic-ZrO_2 and the cubic-In_2O_3 phases. The 90 and 95 m/o $InO_{1.5}$ specimens consisted of the cubic ZrO_2 and the cubic In_2O_3 phases after sintering at 1500°C for 36 h.[12] These results support the conclusion that the minimum at 90 m/o $InO_{1.5}$ and the maximum at 80 m/o $InO_{1.5}$ in electrical conductivity are caused by the supersaturation of ZrO_2 in the In_2O_3. The slow phase separation and the conduction mechanism in the supersaturated 95 m/o specimen both suggest that the Zr^{4+} ions first intend to form defect complexes in the In_2O_3 lattice rather than segregate to form the cubic-ZrO_2 phase as a second phase in the supersaturated single-phase region.

Conclusion

The electrical conductivity in the cubic-ZrO_2 + cubic-In_2O_3 two-phase, and cubic-In_2O_3 single-phase regions of the In_2O_3-ZrO_2 system was measured, in the temperature range between room temperature and 1300°C, and in the oxygen partial pressure range between 5×10^{-5} and 1 atm. In the cubic-ZrO_2 + cubic-In_2O_3 two-phase region, the electrical conductivity of electronic character increases abruptly up to 10^4 Sm^{-1} with increasing $InO_{1.5}$ concentration. This material is a 3D composite of an ionic conductor and an electronic conductor.

In_2O_3 doped with ZrO_2 is a high n-type electronic conductor up to ≈10^5 Sm^{-1} at 1300°C. The highest electrical conductivity was found in the cubic-In_2O_3 solid solution containing 0.5 m/o ZrO_2 near the thermodynamic solubility limit in air. Further addition of ZrO_2 led to a decrease in electronic conductivity in air due to the defect complex formation. The dependences of the electronic conductivity of ZrO_2-doped In_2O_3 on oxygen partial pressure, temperature, and ZrO_2 dopant concentration, can be summarized as that the predominate lattice defects for electronic conduction change from: (*i*) defect complexes (σ is independent of p_{O_2}), to (*ii*) oxygen interstitial-dopant cation neutral pairs (p_{O_2} dependence of power −1/8), (or isolated oxygen interstitials), and (*iii*) free-electrons after reducing oxygen interstitials (σ becomes less dependent on p_{O_2}) with increasing temperature, with decreasing p_{O_2}, and with decreasing dopant concentration, leading to a higher electronic conductivity. The metastable solubility of dopants in In_2O_3 due to the slow phase separation kinetics influences the electronic conductivity and lattice defect mechanisms. ZrO_2 is a most effective donor for increasing electronic conductivity of In_2O_3, among hypervalent metal oxides including SnO_2, Nb_2O_5, and CeO_2. The ZrO_2-doped In_2O_3 therefore has potential use as highly conductive films for various electrical, electrochemical, and optical applications.

Acknowledgment

This study was supported by the Swiss Federal Office of Energy. The authors thank L. Dubal from this office for his

Downloaded on 2014-03-27 to IP 140.120.135.222 address. Redistribution subject to ECS terms of use (see ecsdl.org/site/terms_use) unless CC License in place (see abstract).

support and continuous interest. We thank P. Bohac for his helpful suggestions.

Manuscript submitted Dec. 29, 1993; revised manuscript received May 2, 1994. This was Paper 670 presented at the San Francisco, CA Meeting of the Society, May 22-27, 1994.

Swiss Federal Institute of Technology assisted in meeting the publication costs of this article.

REFERENCES

1. K. Sasaki, P. Bohac, and L. J. Gauckler, *J. Am. Ceram. Soc.*, **76,** 689 (1993).
2. K. Sasaki, Ph.D. Thesis, Swiss Federal Institute of Technology (ETH-Zürich), Switzerland (1993).
3. D. K. Hohnke, *J. Phys. Chem. Solids,* **41,** 777 (1980).
4. A. P. Sellars and B. C. H. Steele, *Mater. Sci. Forum,* **34-36,** 255 (1988).
5. X. Turrillas, A. P. Sellars, and B. C. H. Steele, *Solid State Ionics,* **28-30,** 465 (1988).
6. L. J. Gauckler, K. Sasaki, H. Heinrich, P. Bohac, and A. Orliukas, in *Science and Technology of Zirconia V,* S. P. S. Badwal, M. J. Bannister, and R. H. J. Hannink, Editors, p. 555, Technomic Publishing, PA (1993).
7. T. S. Sheu, Ph.D. Thesis, University of Michigan, Ann Arbor, MI (1989).
8. T. S. Sheu, T. Y. Tien, and I. W. Chen, *J. Am. Ceram. Soc.,* **75,** 1108 (1992).
9. K. Sasaki, A. Orliukas, P. Bohac, and L. J. Gauckler, in *Proceedings of the European Ceramic Society Second Conference,* G. Ziegler and H. Hausner, Editors, p. 2185, Deutsche, Keramische Gesellschaft (1993).
10. Y. Kanai, *Jpn. J. Appl. Phys.,* **23,** 127 (1984).
11. L. V. Morozova, P. A. Tikhonov, A. V. Komarov, V. P. Popov, V. B. Glushkova, and Yu. P. Zarichnyak, *Russ. J. Phys. Chem. (English Translation),* **60,** 853 (1986).
12. L. V. Morozova, P. A. Tikhonov, and V. B. Glushkova, *ibid.,* **64,** 453 (1990).
13. J. L. Bates, C. W. Griffin, D. D. Marchant, and J. E. Garnier, *Am. Ceram. Soc. Bull.,* **65,** 673 (1986).
14. I. Hamberg and C. G. Granqvist, *J. Appl. Phys.,* **60,** R123 (1986).
15. R. Banerjee, D. Das, S. Ray, A. K. Batabyal, and A. K. Barua, *Solar Energy Mater.,* **13,** 11 (1986).
16. A. L. Dawar and J. C. Joshi, *J. Mater. Sci.,* **19,** 1 (1984).
17. M. Marezio, *Acta Crystallogr.,* **20,** 723 (1966).
18. E. C. Subbarao, D. H. Sutter, and J. Hrizo, *J. Am. Ceram. Soc.,* **48,** 443 (1965).
19. G. P. Wirtz and H. P. Takiar, *ibid.,* **64,** 748 (1981).
20. P. A. Cox, W. R. Flavell, and R. G. Egdell, *J. Solid State Chem.,* **68,** 340 (1987).
21. D. J. McDowell, R. W. Scheidecker, and M. F. Berard, *ibid.,* **23,** 357 (1978).
22. W. W. Barker and A. F. Wilson, *J. Inorg. Nucl. Chem.,* **30,** 1415 (1968).
23. J. G. Pepin, E. R. Vance, and G. J. McCarthy, *J. Solid State Chem.,* **38,** 360 (1981).
24. V. N. Shukla and G. P. Wirtz, *J. Am. Ceram. Soc.,* **60,** 253 (1977).
25. M. F. Berard, C. D. Wirkus, and D. R. Wilder, *ibid.,* **51,** 643 (1968).
26. J. C. C. Fan and J. B. Goodenough, *J. Appl. Phys.,* **48,** 3524 (1977).
27. K. Otsuka, T. Yasui, and A. Morikawa, *Bull. Chem. Soc. Jpn.,* **56,** 2161 (1983).
28. J. Berger, I. Riess, and D. S. Tannhauser, *Solid State Ionics,* **15,** 225 (1985).
29. B. C. H. Steele, in *High Conductivity Solid Ionic Conductors,* T. Takahashi, Editor, p. 402, World Scientific, Singapore (1989).
30. M. Kleitz, in *Fundamental Barriers in SOFC Performance,* p. 4, International Energy Agency (1992).
31. S.-S. Liou and W. L. Worrell, in *Proceedings of the First International Symposium on Solid Oxide Fuel Cells,* S. C. Singhal, Editor, PV 89-11, p. 81, The Electrochemical Society Proceedings Series, Pennington, NJ (1989).
32. S.-S. Liou and W. L. Worrell, *Appl. Phys.,* **A49,** 25 (1989).
33. K. Sasaki, M. Gödickemeier, P. Bohac, A. Orliukas, and L. J. Gauckler, in *Proceedings of the Fifth IEA-Workshop on SOFC,* P. Biedermann and B. Krahl-Urban, Editors, p. 187, Jülich, Germany (1993).
34. Y. Takeda, R. Kanno, M. Noda, Y. Tomida, and O. Yamamoto, *This Journal,* **134,** 2656 (1987).
35. H. L. Tuller, in *Nonstoichiometric Oxides,* O. T. Sørensen, Editor, p. 271, Academic Press, New York (1981).
36. E. F. Sverdrup, D. H. Archer, and A. D. Glasser, *Advances in Chemistry Series,* Vol. 90, p. 301 (1969).
37. G. P. Wirtz and H. S. Isaacs, *Solid State Ionics,* **9&10,** 963 (1983).
38. G. Frank and H. Köstlin, *Appl. Phys.,* **A27,** 197 (1982).
39. K. Sasaki, P. Bohac, and L. J. Gauckler, in *Proceedings of the Third International Symposium on Solid Oxide Fuel Cells,* S. C. Singhal and H. Iwahara, Editors, PV 93-4, p. 288, The Electrochemical Society Proceedings Series, Pennington, NJ (1993).
40. K. Sasaki, M. Gödickemeier, P. Bohac, and L. J. Gauckler, in *Annual Report,* p. 4.1, Swiss Federal Office of Energy, Berne, Switzerland (1992).
41. J. A. Allemann, Ph.D. Thesis, (in German), Swiss Federal Institute of Technology (ETH-Zürich), Zürich, Switzerland (1992).
42. D. Kim, *J. Am. Ceram. Soc.,* **72,** 1415 (1989).
43. P. Li and I. W. Chen, Paper SVII-5-93, presented at the 95th Annual Meeting Am. Ceram. Soc., Cincinnati, OH, April 1993.
44. R. L. Jones and D. Mess, *J. Am. Ceram. Soc.,* **75,** 1818 (1992).
45. J. B. Goodenough, J. E. Ruiz-Diaz, and Y. S. Zhen, *Solid State Ionics,* **44,** 21 (1990).
46. Y. Kanai, *Jpn. J. Appl. Phys.,* **24,** L361 (1985).
47. F. A. Kröger, *The Chemistry of Imperfect Crystals,* (2nd Revised ed.), Vol. 2, Imperfection Chemistry of Crystalline Solids, North-Holland, Amsterdam (1974).
48. T. Maruyama, Y. Saito, M. Shinohara, Y. Aoyama, and W. Komatsu, in *Electro-Ceramics and Solid-State Ionics,* H. L. Tuller and D. M. Smyth, Editors, PV 88-3, p. 104, The Electrochemical Society Proceedings Series, Pennington, NJ (1988).
49. J. H. W. deWit, *J. Solid State Chem.,* **20,** 143 (1977).
50. K. Sasaki, H. P. Seifert, and L. J. Gauckler, in *Proceedings of the Second International Symposium on Ionic and Mixed Conducting Ceramics,* T. A. Ramanarayanan, W. L. Worrell and H. L. Tuller, PV 94-12, p. 336, Electrochemical Society Proceedings Series, Pennington, NJ (1994).
51. R. L. Weiher, *J. Appl. Phys.,* **33,** 2834 (1962).
52. W. Hayes and A. M. Stoneham, *Defects and Defect Processes in Nonmetallic Solids,* John Wiley & Sons, New York (1985).
53. A. S. Nowick, in *Diffusion in Crystalline Solids,* G. E. Murch and A. S. Nowick, Editors, p. 143, Academic Press, Orlando, FL (1984).
54. Ph. Parent, H. Dexpert, G. Tourillon, and J. M. Grimal, in *Non-Stoichiometry in Semiconductors,* K. J. Bachmann, H. L. Hwang, and C. Schwab, Editors, p. 301, Elsevier Science Publishers, Amsterdam (1992).
55. S. J. Wen, G. Couturier, J. P. Chaminade, E. Marquestaut, J. Claverie, and P. Hagenmuller, *J. Solid State Chem.,* **101,** 203 (1992).
56. J. H. W. deWit, *ibid.,* **13,** 192 (1975).
57. Z. S. Teweldemedhin, K. V. Ramanujachary, and M. Greenblatt, *ibid.,* **86,** 109 (1990).
58. N. W. Ashcroft and N. D. Mermin, *Solid State Physics,* Chapt. 28, (Intl. ed.), W. B. Saunders Co., Philadelphia (1976).
59. J. H. W. deWit, G. van Unen, and M. Lahey, *J. Phys. Chem. Solids,* **38,** 819 (1977).
60. R. L. Weiher and R. P. Ley, *J. Appl. Phys.,* **37,** 299 (1966).
61. R. L. Weiher and B. G. Dick, Jr., *ibid.,* **35,** 3511 (1964).
62. I. Hamberg, C. G. Granqvist, K. F. Berggren, B. E. Sernelius, and L. Engström, *Phys. Rev.,* **B30,** 3240 (1984).
63. D. Chatterji and R. W. Vest, *J. Am. Ceram. Soc.,* **55,** 575 (1972).
64. C. T. Prewitt, R. D. Shannon, D. B. Rogers, and A. W. Sleight, *Inorg. Chem.,* **8,** 1985 (1969).
65. S. A. Agnihotry, K. K. Saini, T. K. Saxena, K. C. Nagpal, and S. Chandra, *J. Phys. D,* **18,** 2087 (1985).

Downloaded on 2014-03-27 to IP 140.120.135.222 address. Redistribution subject to ECS terms of use (see ecsdl.org/site/terms_use) unless CC License in place (see abstract).